

Sub-Doppler spectroscopy of the PH radical: Hyperfine structure in the $A^3\Pi$ state

James A. J. Fitzpatrick, Oleg V. Chekhlov, and Colin M. Western^{a)}

School of Chemistry, University of Bristol, Cantock's Close Bristol BS8 1TS, United Kingdom

Stephen H. Ashworth

School of Chemical Sciences and Pharmacy, University of East Anglia, Norwich NR4 7TJ, United Kingdom

(Received 8 November 2002; accepted 16 December 2002)

Sub-Doppler spectra of the $A^3\Pi-X^3\Sigma^-(0,0)$ and $(1,0)$ bands of the PH radical have been recorded using an injection seeded single mode optical parametric oscillator in a supersonic jet expansion. Most of the rotational lines in these laser-induced fluorescence spectra exhibit clear splittings or asymmetry due to hyperfine structure. An analysis of this structure is presented in terms of the electronic structure and bonding of the molecule. Comparisons are drawn with the corresponding $A^3\Pi$ state of the NH radical, and some shortcomings in the accepted methods for interpretation are highlighted and discussed. © 2003 American Institute of Physics. [DOI: 10.1063/1.1543946]

I. INTRODUCTION

The hyperfine structure of free-radical spectra is well known as a tool to probe their electronic structure.¹ This structure is typically dominated in radicals by a magnetic interaction between nuclei with nonzero spin and the spin or orbital angular momentum of the unpaired electrons.² Since the experimentally measurable magnetic hyperfine parameters are determined by averages over the wave functions of these electrons, they provide a direct route to investigating the composition of the electronic wave function. Valuable information can be derived such as the *s*-character of the unpaired electrons or the spatial distribution of the unpaired π electron density.³ The recent development in our group of a narrow bandwidth pulsed visible/UV laser system^{4,5} has allowed us to obtain this information for excited states much more easily than before, and this paper presents such a study of the PH radical.

The PH radical is a promising candidate for measuring hyperfine structure, as both nuclei have nonzero spin and phosphorus has a relatively large magnetic moment, which leads to easily resolvable hyperfine structure. The $A^3\Pi-X^3\Sigma^-$ band system was studied previously at Doppler limited resolution by Legay⁶ and Rostas,⁷ who provided rotational and fine structure constants for $v'=0$ and 1. These were refined in our recent spectroscopic study of the predissociation dynamics involving the $(0,0)$, $(1,0)$, and $(2,0)$ bands of the $A^3\Pi-X^3\Sigma^-$ band system.⁸ Most of the rotational lines are absent from the laser-induced fluorescence (LIF) spectrum of the $(1,0)$ band due to a spin-orbit-induced coupling to the repulsive $^5\Sigma^-$ state which correlates with ground-state atomic fragments. This coupling increases with v' and J' , so the $(2,0)$ band is void of any LIF signal except for one strong line with $J'=0$, which is the only line which cannot predissociate directly via the spin-orbit coupling mechanism. The electronic ground state is well understood,

having been studied by laser magnetic resonance (LMR) by Davies *et al.*⁹ and microwave (MW) spectroscopy by Goto and Saito,¹⁰ these have provided accurate ground-state fine and hyperfine structure constants including Fermi contact and nuclear-spin, electron-spin, dipole-dipole coupling constants. There has also been some theoretical interest in calculating selected isotropic and anisotropic hyperfine coupling constants *ab initio* for a range of phosphorus containing radicals including PH.^{11,12} The calculations were restricted to the ground ($X^3\Sigma^-$) electronic state and provided values for the Fermi contact and the dipole-dipole terms in good agreement with experimental observations.

We present here the first measurements of the hyperfine coupling constants for both the phosphorus and hydrogen nuclei in the excited electronic state, along with refined rotational and fine structure constants for the $(0,0)$ band of the $A^3\Pi-X^3\Sigma^-$ system of the PH radical. The bonding in the ground and excited electronic states is then interpreted using these hyperfine parameters and a comparison is drawn with the high-resolution measurements of the $A^3\Pi-X^3\Sigma^-$ band system of the NH radical.¹³

II. EXPERIMENT

The injection seeded OPO system used here to produce narrow bandwidth light will be described only briefly, as its design and performance has been published elsewhere.^{4,5} The system is based on the design of Votava *et al.*¹⁴ and consists of two BBO crystals mounted in a walk-off compensation geometry¹⁵ situated inside a ring cavity defined by four planar mirrors. Three of these mirrors are highly reflective (>99.9%) in a window of 880–1050 nm, and one (the output coupler) is ~85% reflective in the same wavelength range. The crystals were pumped by the third harmonic of an injection seeded Spectra-Physics PRO 190 long pulse Nd:YAG laser. The pump light was coupled in and out of the cavity by two Brewster steering mirrors, which were highly reflective for 355 nm at 56 deg. The seed source was a com-

^{a)}Electronic mail: c.m.western@bristol.ac.uk

mercial external cavity diode laser (Sacher TEC 500) lasing between 930 and 980 nm, which corresponds to a tuning range on the signal wave of 555–575 nm.

One of the highly reflective cavity mirrors was mounted on a piezo-driven mount (PZT), which allowed adjustments to be made to the cavity length to ensure that the cavity was always resonant with the injected seed wavelength. Cavity locking was achieved by the difference polarization locking scheme of Hänsch and Coulliard.¹⁶ The error signal generated by this process was fed to a controlling computer, which in turn controlled the offset of the PZT via a simple feedback algorithm. The algorithm provided discrimination against the saturation of the photodiode during the pump pulse and was able to reset the cavity when the end of the PZT scan range was reached.

Narrow bandwidth UV light in the range of ~ 340 nm was generated by sum frequency mixing of the idler output with 532 nm light from the Nd:YAG pump laser in a KDP crystal. The idler output was focused using a cylindrical lens ($f=25$ cm) in the plane perpendicular to the plane of phase matching. PH radicals were generated in a supersonic jet expansion of 4% PH₃ in Ar at a backing pressure of 1 atmosphere using a pulsed electrical discharge system as described in Ref. 17. Spectra were taken using laser-induced fluorescence with the Doppler width minimized by selectively imaging the fluorescence from the center of the intersection of the laser beam with the supersonic gas expansion.¹⁸ Analysis of the LIF spectra showed the unbroadened rotational lines were represented well by a Lorentzian function with a FWHM of 0.012 cm^{-1} (~ 350 MHz). This linewidth is greater than the bandwidth of the UV light, and is consistent with a width of ~ 130 MHz from the frequency mixed UV and ~ 270 MHz from a residual Doppler width at ~ 20 K. The signal from the PMT was then recorded via a digital oscilloscope on to a computer for data acquisition. A portion of the seed light was directed to a commercial Lambdameter (Cluster LM-007), which measured the wavelength of the idler wave and consequently allowed the generation of an accurate frequency scale. Note that relative frequencies were determined rather more accurately than absolute positions because of the details of the way the spectra were recorded. One limitation is not imaging the exact center of the supersonic jet expansion leading to a systematic

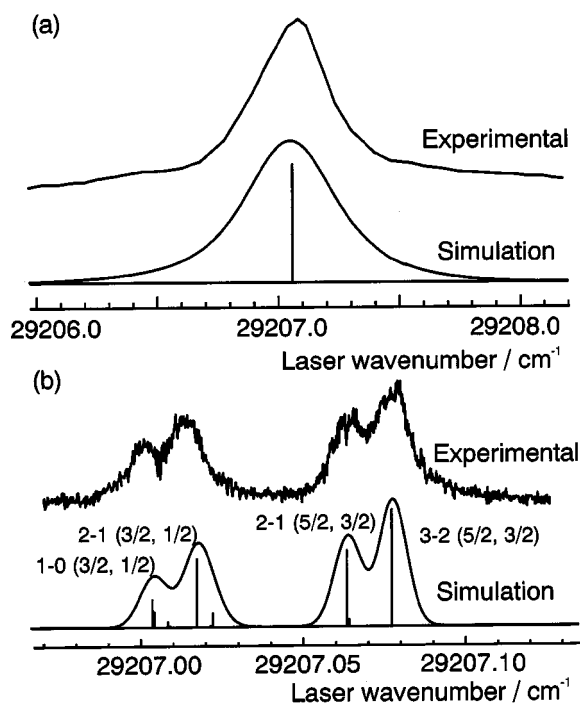


FIG. 1. (a) A normal resolution ($\sim 0.2\text{ cm}^{-1}$) dye laser scan of a single rotational line ($J=2$) from the F_1 component. (b) A high-resolution OPO scan revealing the underlying hyperfine structure. The notation used for the quantum numbers (as defined in the text) is $F' - F''(F'_1 - F''_1)$.

Doppler shift in all the spectra. A drift in the frequency of the (stabilized) seed laser of the pump YAG would have a similar effect. Tests have indicated both these effects to be small, but this does reduce the precision with which we can quote band origins. It does not affect any of the other parameters which are all determined from frequency differences.

III. RESULTS AND ANALYSIS

The (0,0) band of the $A^3\Pi - X^3\Sigma^-$ system was recorded at sub-Doppler resolution at $\sim 29\,500\text{ cm}^{-1}$ [a low- and high-resolution scan is illustrated in Figs. 1(a) and 1(b)]. Initially, the rotational line positions were fitted to the Hamiltonian¹⁹

$$\begin{aligned} \hat{H}_{\text{rot}} = & B\hat{N}^2 - D\hat{N}^4 + H\hat{N}^6 + L\hat{N}^8 + A\hat{L}\cdot\hat{S} + \gamma\hat{N}\cdot\hat{S} + \frac{1}{2}\gamma_D[\hat{N}\cdot\hat{S}, \hat{N}^2]_+ + \frac{2}{3}\lambda(3\hat{S}_z^2 - \hat{S}^2) + \frac{1}{2}\lambda_D[\frac{2}{3}(3\hat{S}_z^2 - \hat{S}^2), \hat{N}^2]_+ \\ & - \frac{1}{2}p(\hat{N}_+\hat{S}_+e^{-2i\phi} + \hat{N}_-\hat{S}_-e^{+2i\phi}) + \frac{1}{2}q(\hat{N}_+^2e^{-2i\phi} + \hat{N}_-^2e^{+2i\phi}) + \frac{1}{2}o(\hat{S}_+^2e^{-2i\phi} + \hat{S}_-^2e^{+2i\phi}) \\ & + \frac{1}{4}q_D[\hat{N}_+^2e^{-2i\phi} + \hat{N}_-^2e^{+2i\phi}, \hat{N}^2]_+, \end{aligned} \quad (1)$$

where $[\hat{A}, \hat{B}]_+ = \hat{A}\hat{B} + \hat{B}\hat{A}$. To fit all the observed transitions to within the accuracy of the Lambdameter ($\sim 0.003\text{ cm}^{-1}$), a number of centrifugal distortion corrections to the lower and upper state rotational and fine structure constants had to be included. Only the upper state rotational and fine structure

constants along with the first-order centrifugal distortion corrections to B' and γ' were included in the line position fit. This yielded an improved set of rotational and fine structure constants with respect to Ref. 8 which is quoted in Table I. Several unpredissociated lines from the (1,0) band were also

TABLE I. Rotational and fine structure constants for the $v' = 0X^3\Sigma^-$ (Ref. 10) and $A^3\Pi$ states of PH.

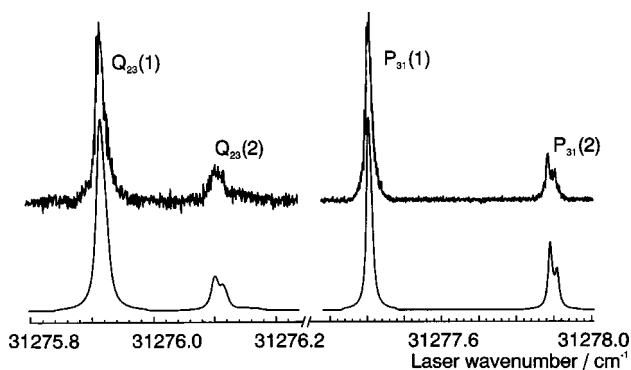
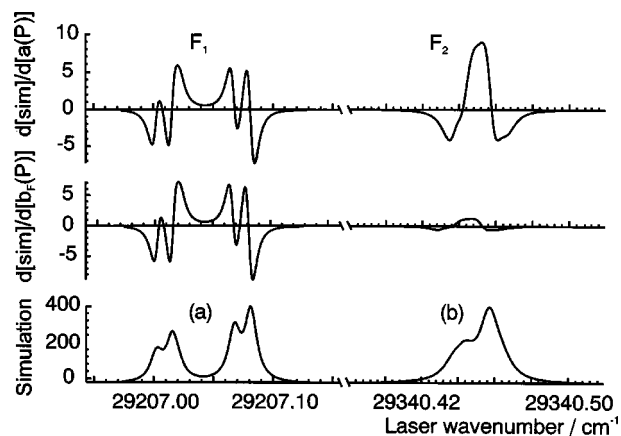
Parameter [cm ⁻¹]	$X^3\Sigma^-$ ^a	$A^3\Pi$
Origin	...	29 311.82 ^b
B	8.412 514	8.026 90 (79) ^c
$D \times 10^4$	4.437	3.16 (67)
$H \times 10^8$	1.39	...
$L \times 10^{11}$	0.5	...
A	...	-115.653 7 (71)
λ	2.210 052	1.000 7 (20)
$\lambda_D \times 10^7$	19.0	...
γ	-0.076 906	0.020 8 (61)
$\gamma_D \times 10^7$	1.42	188.3 (32)
o	...	-0.145 34 (18)
p	...	0.070 0 (16)
q	...	-0.007 8 (59)

^aConstants from Ref. 10.^bWe quote no error bar here due to the possible systematic uncertainties in the frequency positions as discussed in the Experiment section.^cFigures in parentheses denote one standard deviation in units of the last decimal place.

recorded at sub-Doppler resolution (Fig. 2). As discussed in the Introduction, the majority of the lines was missing from this band, so a fit was not undertaken.

As the lines in the electronic spectrum were widely spaced, a selection of rotational lines from each spin-orbit component were each scanned several times individually to provide a number of alternate scans to fit and extract the hyperfine constants. Since there have been no previously reported hyperfine parameters for the $A^3\Pi$ state of PH, initial guesses for the nuclear spin-orbit and Fermi contact coupling constants were made by assuming percentages of appropriate atomic expectation values of $\langle r^{-3} \rangle$ (100% on P and 0% on H) and $|\Psi_0|^2$ (50% on each of P and H) from Morton and Preston.²⁰ This initial set of hyperfine constants allowed the reproduction of the general appearance of the experimental spectrum. These constants were then refined in a line position fit along with the rotational and fine structure constants using a Hamiltonian with a rotational part and a hyperfine part

$$\hat{H} = \hat{H}_{\text{rot}} + \hat{H}_{\text{hyp}}(\text{P}) + \hat{H}_{\text{hyp}}(\text{H}), \quad (2)$$

FIG. 2. A high-resolution scan of the unpredissociated F_3 , e parity lines in the (1,0) band of the $A^3\Pi-X^3\Sigma^-$ transition in PH.FIG. 3. The numerical derivative of the simulation with respect to the a and b_F hyperfine constants for phosphorus for two different rotational lines. (a) $J=2$, F_1 and (b) $J=1$, F_2 .

with \hat{H}_{rot} as is defined in Eq. (1). The hyperfine part takes the following form for both nuclei:²¹

$$\begin{aligned} \hat{H}_{\text{hyp}} = & a\hat{I}_z\hat{L}_z + b_F\hat{\mathbf{I}}\cdot\hat{\mathbf{S}} + \frac{1}{3}c(3\hat{I}_z\hat{L}_z - \hat{\mathbf{I}}\cdot\hat{\mathbf{S}}) \\ & + d(\hat{S}_+\hat{I}_+e^{-2i\phi} + \hat{S}_-\hat{I}_-e^{+2i\phi}). \end{aligned} \quad (3)$$

The angular momenta are coupled together in a parity conserved Hund's case a_β basis

$$\hat{\mathbf{F}}_1 = \hat{\mathbf{J}} + \hat{\mathbf{I}}_P; \quad \hat{\mathbf{F}} = \hat{\mathbf{F}}_1 + \hat{\mathbf{I}}_H, \quad (4)$$

and the energy levels were calculated by diagonalizing the Hamiltonian [Eq. (2)] using a basis containing all J and F_1 for a given F .

Approximate values for a and b_F could be obtained from a line position fit to this Hamiltonian. These were then refined by fitting the line contours of the rotational line shapes to the simulated profiles.²² A combined fit to all the line profiles simultaneously gave poor results, so individual fits were performed to no more than one or two line profiles at any one time. There is not sufficient information in individual profiles to determine more than one or two parameters, but this is in fact not a problem because most line profiles are mainly sensitive to a single combination of parameters for each nucleus. As the A state is essentially Hund's case b, it is not clear from the Hamiltonian [Eq. (3)] which combination of parameters is important for any given rotational state. We therefore took numerical derivatives of the simulated spectra with respect to each parameter. A sample is illustrated in Fig. 3, from which it can be seen that splittings in the $J=1$, F_2 component are strongly dependent on $a(\text{P})$ but not $b_F(\text{P})$, while in the $J=2$, F_1 component a key quantity is $\sim a + b$. Repeating the process for all the magnetic parameters yields Table II, which leads to a sequence of determinations of b_F and d (from F_3 lines), then a (from F_2 lines keeping b_F , c , and d fixed), then c (from F_1 lines keeping a , b_F , and d fixed). The individual rotational lines used in each case are shown in Table II. The procedure is repeated to ensure consistency, and the final results are shown in Table III, where the standard deviations are estimated from the consistency between fits to four independent sets of spectra.

TABLE II. Indication of which hyperfine constants influence the form of the rotational lines from each spin-orbit component.

Parameter	Influences	Fit 1	Fit 2	Fit 3
a	F_1 F_2	$P_{21}(2), R_{23}(0), Q_{21}(1), Q_{21}(2), R_{21}(1)$...
b_F	F_1 ... F_3	$P_{32}(1), Q_{32}(1), P_{31}(1), Q_{31}(1), R_{32}(1)$
c	F_1	$R_{12}(1), Q_{11}(2), R_{11}(1), R_{11}(2)$
d	... F_2 F_3	$P_{32}(1), Q_{32}(1), P_{31}(1), Q_{31}(1), R_{32}(1)$

We believe this fit to be unique, in that the same final values were obtained from several different starting points on different sets of data. A partial check is available from the observed hyperfine structure of the unpredissociated rotational lines from $v'=1$ in the $A^3\Pi$ state shown in Fig. 2. The simulation shown used the fitted hyperfine constants from $v'=0$. It is clear that this provides a good fit to the spectrum, suggesting little change in the hyperfine constants upon vibrational excitation. This in turn suggests there is little change in the bonding character, consistent with the small change in the average internuclear separation between $v'=0$ and 1.

IV. DISCUSSION

It is now possible to discuss the electronic structure of PH as all experimentally measurable magnetic hyperfine parameters are defined as averages over the electronic wave function,²³

$$a = 2g_N\mu_B\mu_N \frac{1}{\Lambda} \langle nS\Lambda\Sigma | \sum_j \frac{\hat{l}_{jz}}{r_j^3} | nS\Lambda\Sigma \rangle, \quad (5)$$

$$b_F = \frac{8\pi}{3} g_S g_N \mu_B \mu_N \frac{1}{\Sigma} \langle nS\Lambda\Sigma | \sum_j \delta(\hat{\mathbf{r}}_j - \hat{\mathbf{C}}) \hat{s}_{jz} | nS\Lambda\Sigma \rangle, \quad (6)$$

$$c = \frac{3}{2} g_S g_N \mu_B \mu_N \frac{1}{\Sigma} \langle nS\Lambda\Sigma | \sum_j \frac{(3 \cos^2 \theta_j - 1) \hat{s}_{jz}}{r_j^3} | nS\Lambda\Sigma \rangle, \quad (7)$$

TABLE III. Hyperfine structure constants for the $X^3\Sigma^-$ (Ref. 10) and $A^3\Pi$ states of PH.

Parameter [cm^{-1}]	$X^3\Sigma^-$ ^a	$A^3\Pi$
$a(\text{P})$...	0.020 26(20) ^b
$b_F(\text{P})$	0.004 253	0.042 62(62)
$c(\text{P})$	-0.015 906	0.000 44(8)
$d(\text{P})$...	0.018 32(41)
$a(\text{H})$...	-0.003 01(48)
$b_F(\text{H})$	-0.001 551	0.019 6(12)
$c(\text{H})$	0.000 647	-0.012 52(33)
$d(\text{H})$...	0.000 2(35)

^aConstants from Ref. 10.

^bFigures in parentheses denote one standard deviation in units of the last decimal place.

$$d = -\frac{3}{2} \frac{g_S g_N \mu_B \mu_N}{\sqrt{S(S+1) - \Sigma(\Sigma+1)}} \times \langle nS\Lambda - 1; \Sigma + 1 | \sum_j \frac{\sin^2 \theta_j e^{-2i\phi_j} \hat{s}_{j+}}{r_j^3} | nS\Lambda + 1; \Sigma \rangle, \quad (8)$$

where μ_B and μ_N are the Bohr and nuclear magnetons, g_S and g_N are the free electron and nuclear spin g -factors, respectively, and (r_j, θ_j, ϕ_j) are the spherical polar coordinates of electron j with respect to the nuclear center under consideration. The delta function in Eq. (6) is only nonzero at the nuclear center C . In these expressions the electronic angular momentum operators have been left in to make clear the differences between the various averages. It is clear, for example, that the summations need only be taken over the unpaired electrons due to the presence of the \hat{l}_z and \hat{s}_z operators in each expression, which will mean that any electrons which are spin-paired will have a net contribution of zero. Note that our definition of the d term is a generalization of the Kristiansen and Veseth term which is specific to doublet states. Once the relevant substitutions have been made, both definitions are consistent.

To rationalize the hyperfine parameters, we shall start by assuming that both the $X^3\Sigma^-$ and $A^3\Pi$ states are well described by single electronic configurations

$$X^3\Sigma^-: \dots 4\sigma^2 1\pi^4 5\sigma^2 2\pi^2,$$

$$A^3\Pi: \dots 4\sigma^2 1\pi^4 5\sigma^1 2\pi^3,$$

and consider the constants in turn.

A. Fermi contact interaction

The Fermi contact interaction [Eq. (6)] is a powerful tool for the determination of the s -character of the unpaired electron density as the matrix element involves only unpaired electrons which have density at the nucleus. Comparing b_F for hydrogen to the known²⁴ value of the wave function at the nucleus of an isolated hydrogen atom, a percentage of the $1s$ character due to unpaired electrons can be obtained. For the excited state this gives a ratio of 40% (Table IV). This must come from σ orbitals, and the simple molecular orbital picture would predict 50% s -character for the 5σ orbital given that it is a $p\sigma$ bonding orbital. The difference is significant, suggesting that some of the hydrogen s -character needs to be assigned to a filled molecular orbital, the most likely one involving the $3s$ orbital on phosphorus. The corresponding derived value for phosphorus using the atomic value from Morton and Preston²⁰ is $\sim 9\%$, while the simple

TABLE IV. Derived percentages of the spatial distribution of π electron density and the s -character of the unpaired electrons in the $X^3\Sigma^-$ and $A^3\Pi$ states of the NH and PH radicals using the atomic values from Morton and Preston (Ref. 20) and from Bunge *et al.* (Ref. 26).

	Morton and Preston				Bunge <i>et al.</i>			
	$X^3\Sigma^-$		$A^3\Pi$		$X^3\Sigma^-$		$A^3\Pi$	
	P	H	P	H	P	H	P	H
$a/\langle r^{-3} \rangle_{\text{atomic}} \times 100$	66.2	84.9	...
$c/\langle r^{-3} \rangle_{\text{atomic}} \times 100$	-52.0	...	1.4	...	-66.6	...	1.8	...
$d/\langle r^{-3} \rangle_{\text{atomic}} \times 100$	58.0	74.3	...
$b_F/b(s)_{\text{atomic}} \times 100$	1.0	-3.3	9.6	41.4

	$X^3\Sigma^-$		$A^3\Pi$		$X^3\Sigma^-$		$A^3\Pi$	
	N	H	N	H	N	H	N	H
	$a/\langle r^{-3} \rangle_{\text{atomic}} \times 100$	64.6	75.0
$c/\langle r^{-3} \rangle_{\text{atomic}} \times 100$	-47.78	...	11.0	...	-55.5	...	12.7	...
$d/\langle r^{-3} \rangle_{\text{atomic}} \times 100$	47.8	55.5	...
$b_F/b(s)_{\text{atomic}} \times 100$	1.1	-4.7	8.8	21.2

molecular orbital picture would predict no s -character as the 5σ orbital is a $p\sigma$ orbital located on phosphorus. This also suggests that the orbital is better described as an sp -hybrid rather than a pure $p\sigma$ orbital.

The corresponding values in the ground state are both small, consistent with all the σ orbitals being filled. An additional mechanism must be invoked to account for the negative values found for hydrogen. This is essentially a correlation effect, with the two unpaired electrons in the 2π orbital causing a distortion of the spin density in the filled orbitals. This mechanism, known as spin-polarization, is well known and typically leads to small negative Fermi contact coupling constants for protons and small positive constants for heavier nuclei,³ as is found here in the constants obtained from the MW study of Goto and Saito.¹⁰

B. Nuclear spin–electron orbit interaction

Comparison of a [Eq. (5)] with atomic values of $\langle r^{-3} \rangle$ allows the derivation of the unpaired π electron density at phosphorus. The atomic expectation value of $\langle r^{-3} \rangle$ used for the comparison was initially taken from the accepted values for interpretation of Morton and Preston²⁰ calculated using the Herman and Skillman method.²⁵ The molecular orbital picture predicts that the 2π orbital is localized solely on phosphorus so values close to 100% might be expected. From Table IV, it can be seen that the actual value is only $\sim 70\%$ and it is hard to see what mixing could reduce the value from 100%. However, the Herman–Skillman method is limited in that it relies on an approximate local treatment of the exchange term. If we use an alternate set of atomic expectation values calculated using the more accurate standard Hartree–Fock methods by Bunge *et al.*,²⁶ the percent-

age increases to $\sim 85\%$, in reasonable agreement with the zeroth-order picture. The possibility of whether more accurate atomic calculations would make a difference to the interpretation is discussed later. It does, however, suggest shortcomings in the use of the Morton and Preston values in providing a satisfactory basis for the interpretation of the experimental hyperfine constants. Note that a simple interpretation of the a constant obtained for the hydrogen nucleus is not possible (as discussed by Hirota³) as it is dominated by the effects of the adjacent atom.

C. Nuclear spin–electron spin dipolar interaction

In contrast to a and b_F , the c dipole–dipole interaction [Eq. (7)] involves an angular factor. This angular factor will depend on the orientation of the orbitals and will be different for $p\sigma$ and $p\pi$. These factors can be easily calculated if we assume hydrogenic p orbitals, and the results for various open-shell configurations are given in Table V. The observed ratios are given in Table IV. From this, we can see that the ratios for the excited state are much smaller than the 30% predicted for the simple molecular orbital picture (in this case the differences between the two sources for atomic values of $\langle r^{-3} \rangle$ is less significant). This again suggests that the 5σ orbital is actually an sp -hybrid because the angular factor for an atomic s orbital is zero, and consequently, any increase in the s -character of the orbital means the measured angular factor is reduced from that expected for a pure $p\sigma$ orbital. The ratios for the ground state are broadly in line with the 60% prediction of the simple molecular orbital picture.

The d dipolar term [Eq. (8)] is slightly more difficult to interpret as it is an off-diagonal matrix element. The only

TABLE V. Calculated angular factors for c dipolar term assuming various open-shell electronic configurations.

Configuration	State	Factor
$ \pi_\alpha^+ \pi_\alpha^- $	$^3\Sigma^-$	-3/5
$ \pi_\alpha^+ \sigma_\alpha $	$^3\Pi$	3/10

TABLE VI. Ratios of hyperfine constants for phosphorus and nitrogen.

$A^3\Pi$	a/d	$a/\frac{10}{3}c$
P	1.11(2)	13.8(6) ^a
N	1.35(3)	1.77(6)

^aFigures in parentheses denote one standard deviation in units of the last decimal place.

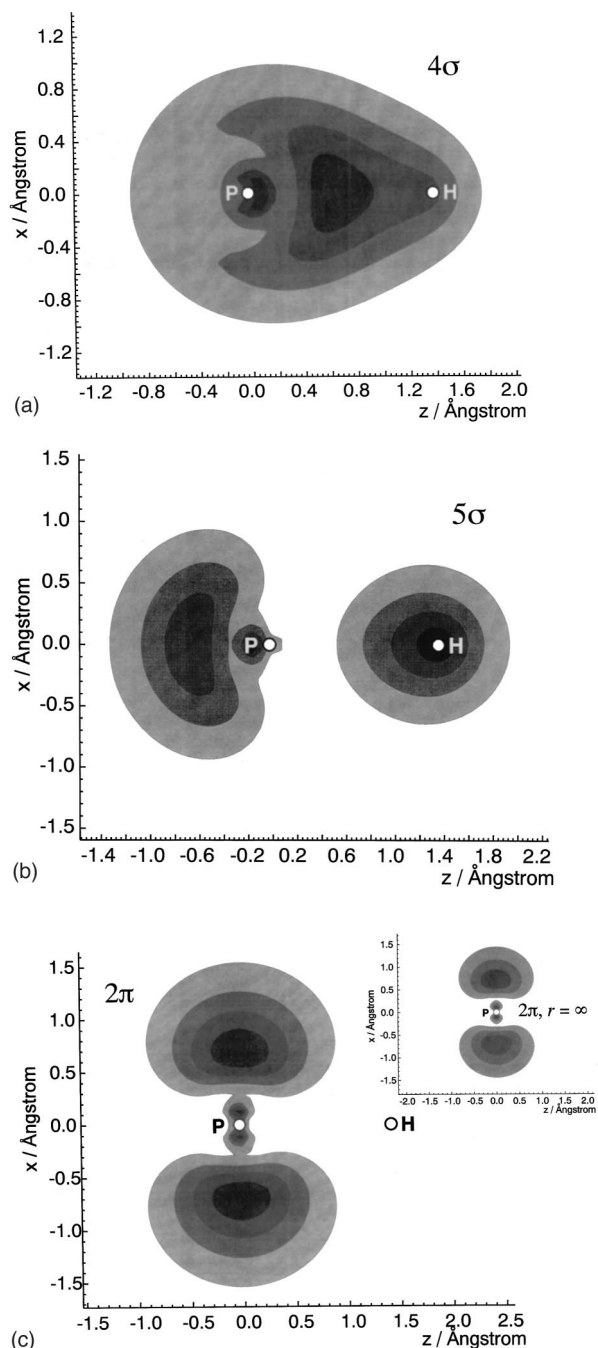


FIG. 4. *Ab initio* Hartree-Fock molecular orbitals (a) 4σ , (b) 5σ , and (c) 2π calculated with an uncontracted cc-pV6Z basis set. The orbital inset in (c) shows an atomic $3p$ orbital of phosphorus calculated using the same level of theory and basis set.

nonzero contributions will come from unfilled π orbitals in the Π electronic state, and for the expected A state configuration of $\pi_{\alpha}^{\dagger}\sigma_{\alpha}$ the angular factor derived using the same logic as for the c term would be 1. As a result we expect (as for a) ratios of 100% for phosphorus. Table IV shows that even with our preferred atomic values from Bunge *et al.*²⁶ the ratio is only 75%. This value seems rather low, and sp -hybridization would not change this value, so it may be that other configurations need to be considered. The question of whether or not the accuracy of the atomic values used for comparison is important can be investigated by using the

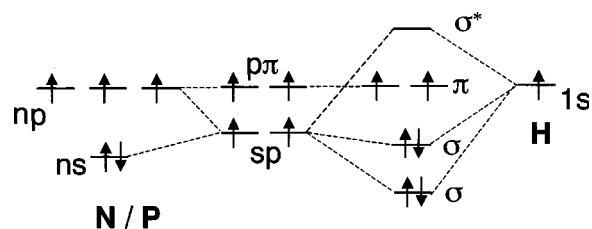


FIG. 5. Molecular orbital diagram illustrating the sp hybridization effects on phosphorus.

logic of Varberg *et al.*²⁷ to establish a relationship between the three constants (a , c , and d) which is independent of $\langle r^{-3} \rangle$

$$a = \frac{10}{3}c = d. \quad (9)$$

It can be seen from Table VI that this relationship is only approximately true, so the uncertainty in the atomic values does not account for the whole discrepancy.

D. Electronic structure from hyperfine interactions

The magnetic hyperfine constants [Eqs. (5)–(8)] have enabled detailed information about the electronic structure of PH to be derived, and this can be compared with the results of *ab initio* calculations. Figure 4 shows molecular orbitals calculated with Hartree-Fock theory by MOLPRO²⁸ using the correlation-consistent basis sets of Dunning *et al.*^{29,30} Figure 4(c) shows the 2π molecular orbital and the same orbital calculated at large r and there is no obvious difference, again consistent with the $\sim 90\%$ $p\pi$ character on phosphorus inferred from the a constant. Figures 4(a) and 4(b) show the 4σ and 5σ molecular orbitals; clearly, the 4σ orbital is not a $3s$ orbital on phosphorus and the lack of electron density between phosphorus and hydrogen in the 5σ orbital is not characteristic of a $p\sigma$ bonding orbital. The calculated orbitals could be generated if we invoke strong mixing between the $3s$ and $3p$ orbitals on phosphorus making two sp hybrids. This is entirely consistent with the reduced s -character on hydrogen and the relatively low values for c . A revised molecular orbital diagram is shown in Fig. 5, reflecting these changes.

E. Comparison between PH and NH

As hyperfine constants are available¹³ for the corresponding state in NH, it is instructive to apply the above analysis to NH. Tables IV and VI include the ratios for NH and, as might be expected, the pattern of results is broadly similar. Most notable is the difference when comparing a and d constants to the expectation values of $\langle r^{-3} \rangle$. Again, the Morton and Preston atomic values give ratios that seem unrealistically low, but even when the Bunge *et al.* atomic values are used, there is still a significant difference between the derived value of $\sim 75\%$ and $\sim 56\%$ with the expected value of 100%. The ratios for c and b_F show some difference, but this can simply be explained by a difference in the degree of sp -hybridization.

Preliminary *ab initio* calculations in NH suggest that, as for PH, the π molecular orbital is very similar to that of the

atom. This suggests that more work needs to be undertaken on the atomic values used for comparison; effects such as electron correlation may be more significant for these constants than, for example, the <5% contribution to b_F . The biggest problems seem to be in the excited electronic states, so the interpretation of previous microwave studies on ground states is not much affected. We are currently undertaking high-level *ab initio* calculations of both atomic and molecular hyperfine coupling constants, and a discussion of these will be presented later.

V. CONCLUSIONS

We present the first measurements of hyperfine coupling constants for the excited $A^3\Pi$ state of PH which have enabled detailed information about the electronic wave function of PH in the excited electronic state to be extracted. Comparison with similar information available for the same excited electronic state of the NH radical indicates broad similarities in the electronic structure with some differences in the detail. The analysis of the hyperfine constants has also indicated some shortcomings in the interpretation, partly due to the limitations in the atomic values used for comparison.

ACKNOWLEDGMENTS

The authors wish to acknowledge EPSRC for funding equipment, a postdoctoral fellowship (O.V.C.), and a Ph.D. studentship (J.A.J.F.). We would also like to acknowledge Spectra-Physics for financial and technical support, Keith Rosser for his expert assistance in maintaining the experimental apparatus, and Robin Griffin and Gareth Elliott for their assistance in taking some of the experimental spectra.

¹W. Gordy and R. L. Cook, *Microwave Molecular Spectra* (Wiley, New York, 1984).

²C. H. Townes and A. L. Schawlow, *Microwave Spectroscopy* (Dover, New York, 1975).

³E. Hirota, *High-Resolution Spectroscopy of Transient Molecules*, Number 40 in Springer Series in Chemical Physics (Springer, Berlin, 1985).

- ⁴J. A. J. Fitzpatrick, O. V. Chekhlov, J. M. F. Elks, C. M. Western, and S. H. Ashworth, *J. Chem. Phys.* **115**, 6920 (2001).
- ⁵O. V. Chekhlov, J. A. J. Fitzpatrick, K. N. Rosser, S. H. Ashworth, and C. M. Western, *J. Mod. Opt.* **49**, 865 (2002).
- ⁶F. Legay, *Can. J. Phys.* **38**, 797 (1960).
- ⁷J. Rostas, D. Cossart, and J. B. Bastien, *Can. J. Phys.* **52**, 1274 (1974).
- ⁸J. A. J. Fitzpatrick, O. V. Chekhlov, D. R. Morgan, R. W. Burrows, and C. M. Western, *Phys. Chem. Chem. Phys.* **4**, 1114 (2002).
- ⁹P. B. Davies, D. K. Russell, and B. A. Thrush, *Chem. Phys. Lett.* **36**, 280 (1975).
- ¹⁰M. Goto and S. Saito, *Chem. Phys. Lett.* **211**, 443 (1993).
- ¹¹M. T. Nguyen, S. Creve, L. A. Eriksson, and L. G. Vanquickenbourne, *Mol. Phys.* **91**, 537 (1997).
- ¹²M. T. Nguyen, S. Creve, and L. G. Vanquickenbourne, *J. Phys. Chem. A* **101**, 3174 (1997).
- ¹³W. Ubachs, J. J. ter Meulen, and A. Dymanus, *Can. J. Phys.* **62**, 1374 (1984).
- ¹⁴O. Votava, J. R. Fair, D. F. Plusquellic, E. Riedle, and D. J. Nesbitt, *J. Chem. Phys.* **107**, 8854 (1997).
- ¹⁵W. R. Bosenberg and D. R. Guyer, *Appl. Phys. Lett.* **61**, 387 (1992).
- ¹⁶T. W. Hansch and B. Couillard, *Opt. Commun.* **35**, 441 (1980).
- ¹⁷K. N. Rosser, Q.-Y. Wang, and C. M. Western, *J. Chem. Soc., Faraday Trans.* **89**, 391 (1993).
- ¹⁸T. J. Slotterback, S. G. Clement, K. C. Janda, and C. M. Western, *J. Chem. Phys.* **103**, 9125 (1995).
- ¹⁹E. Hirota, J. M. Brown, J. T. Hougen, T. Shida, and N. Hirota, *Pure Appl. Chem.* **66**, 571 (1994).
- ²⁰J. R. Morton and K. F. Preston, *J. Magn. Reson.* (1969-1992) **30**, 577 (1978).
- ²¹R. A. Frosch and H. M. Foley, *Phys. Rev.* **88**, 1337 (1952).
- ²²T. J. Slotterback, S. G. Clement, K. C. Janda, and C. M. Western, *J. Chem. Phys.* **101**, 7221 (1994).
- ²³P. Kristiansen and L. Veseth, *J. Chem. Phys.* **84**, 2711 (1986).
- ²⁴W. Weltner, *Magnetic Atoms and Molecules* (Van Nostrand Reinhold, New York, 1983).
- ²⁵F. Herman and S. Skillman, *Atomic Structure Calculations* (Prentice-Hall, Englewood Cliffs, NJ, 1963).
- ²⁶C. F. Bunge, J. A. Barrientos, and A. V. Bunge, *At. Data Nucl. Data Tables* **53**, 113 (1993).
- ²⁷T. D. Varberg, R. W. Field, and A. J. Merer, *J. Chem. Phys.* **95**, 1563 (1991).
- ²⁸R. D. Amos, A. Bernhardsson, A. Berning *et al.*, MOLPRO, a package of *ab initio* programs designed by H.-J. Werner and P. J. Knowles, version 2002.1, 2002.
- ²⁹T. H. Dunning, *J. Chem. Phys.* **90**, 1007 (1989).
- ³⁰D. E. Woon and T. H. Dunning, *J. Chem. Phys.* **98**, 1358 (1993).